Article

Marine Bacterial Chemoresponse to a Stepwise Chemoattractant Stimulus

Li Xie,[1] Chunliang Lu,[2] and Xiao-Lun Wu[1,*]
[1]Department of Physics and Astronomy and [2]Department of Radiology, University of Pittsburgh, Pittsburgh, Pennsylvania

ABSTRACT We found recently that polar flagellated marine bacterium *Vibrio alginolyticus* is capable of exhibiting taxis toward a chemical source in both forward and backward swimming directions. How the microorganism coordinates these two swimming intervals, however, is not known. The work presented herein is aimed at determining the response functions of the bacterium by applying a stepwise chemoattractant stimulus while it is swimming forward or backward. The important finding of our experiment is that the bacterium responds to an identical chemical signal similarly during the two swimming intervals. For weak stimuli, the difference is mainly in the amplitudes of the response functions while the reaction and adaptation times remain unchanged. In this linear-response regime, the amplitude in the forward swimming interval is approximately a factor of two greater than in the backward direction. Our observation suggests that the cell processes chemical signals identically in both swimming intervals, but the responses of the flagellar motor to the output of the chemotaxis network, the regulator CheY-P concentration, are different. The biological significance of this asymmetrical response in polar flagellated marine bacteria is discussed.

INTRODUCTION

Marine bacterium *Vibrio alginolyticus* is capable of swimming in both forward and backward directions propelled by the counterclockwise (CCW) and clockwise (CW) rotations of a polar flagellar motor. At the beginning of each forward interval, the cell randomizes its swimming direction by a flick at the base of the flagellum (1). Such a run-reverse-flick swimming pattern allows the microorganism to perform chemotaxis at a nearly 100% duty cycle, likely improving its fitness in a marine environment. However, aside from swimming interval statistics that had been carefully quantified (2), not much is known about how the forward and backward swimming intervals are regulated by the chemotaxis network. How does the bacterium respond to an identical signal when the motor is in the CCW or CW direction? What are the causes for the difference, if any? And what are the biological implications? These are the issues that we attempt to address in this article.

In a previous study using optical trapping, we determined the overall chemotactic response of *V. alginolyticus* (3). The response function in this case is the total switching rate k_T, which is the mean of the switching rates from CCW to CW (k_f) and from CW to CCW (k_b), after an impulsive chemoattractant stimulus is applied. It was found that the response function is biphasic; i.e., k_T is depressed shortly after the stimulation; it then increases rapidly, overshooting its prestimulation value k_0; and it finally plateaus to a steady-state value k_∞. For a low level of stimulation, k_∞ closely matches k_0, indicating that adaptation of this bacterium is precise. The observed behaviors are similar to what was seen in *Escherichia coli* except that in *E. coli* the response is measured in terms of motor bias instead of the overall switching rate $k_T(t)$ (4). We note that this difference is important because the marine bacterium is capable of performing chemotaxis when the flagellar motor is in either direction, leaving the motor bias more or less constant. This apparent symmetry in CCW and CW motor rotation raises the interesting question of whether the cell differentiates its swimming direction during chemotaxis.

The purpose of this investigation is to study how *V. alginolyticus* responds to chemoattractant stimulation in the forward and backward intervals, separately. For this purpose conditional statistics are collected for those bacteria that swim forward and backward when an identical stepwise stimulus is applied. The investigation is made possible by the use of photolabile NPE-caged-serine, which is biochemically inert until it is converted to a free form of serine upon a short exposure to near ultra-violet (UV) light (5). The caged serine allows uniform stimulation to a population of cells with precise timing and dosage control. The time-dependent, population-averaged switching rates $k_f(t)$ (CCW to CW) and $k_b(t)$ (CW to CCW) are then determined by video microscopy. Unlike the previous study (3), the conditional measurements permit the forward $R_f(t)$ and backward $R_b(t)$ response functions to be determined. It is shown that while $R_f(t)$ and $R_b(t)$ have similar temporal behaviors, the amplitude of $R_f(t)$ is nearly twice as big as $R_b(t)$. The biological and ecological significance of such response functions is then discussed at the end of this work.

Submitted October 23, 2014, and accepted for publication November 24, 2014.

*Correspondence: xlwu@pitt.edu

Editor: Dennis Bray.

0006-3495/15/02/0766/9 $2.00

http://dx.doi.org/10.1016/j.bpj.2014.11.3479

MATERIALS AND METHODS

Bacterial cultures and chemicals

A colony of YM4 was grown at 30°C with vigorous shaking at 200 rpm overnight in LBS medium (1% polypeptone, 0.5% yeast extract, 3% NaCl) (6). The saturated overnight culture was diluted 1:100 into the minimum medium (0.3 M NaCl, 10 mM KCl, 2 mM K_2HPO_4, 0.01 mM $FeSO_4$, 15 mM $(NH_4)_2$ SO_4, 5 mM $MgSO_4$, 1% glycerol, and 50 mM Tris-HCl (pH 7.5)) and grown to an O.D. of 0.2 (7). A 1.5 mL culture was harvested and spun down at 2000 × *g* for 3 min. After removing the supernatant, 1 mL TMN motility medium (50 mM Tris-HCl (pH 7.5), 5 mM $MgCl_2$, 5 mM glucose, 30 mM NaCl, and 270 mM KCl) was used to resuspend the culture, followed by a 5-min centrifuging at 500 × *g* (6). 300–400 μL supernatant was then carefully diluted into 2 mL TMN and shaken at 200 rpm at room temperature for at least half an hour.

NPE-caged-HPTS (8-hydroxypyrene-1,3,6-*tris*-sulfonic acid-8-1-(2-nitrophenyl)ethyl ether) was purchased from Tocris Bioscience (Ellisville, MO) to calibrate the photorelease of NPE-caged-serine. It is nonfluorescent until the fluorescent dye HPTS is uncaged from the protective NPE group when exposed to UV light. NPE-caged-serine (*N*-1-(2-nitrophenyl) ethoxycarbonyl-L-serine) was synthesized according to the reported method in Khan et al. (5). Immediately before the experiment, 5 μL cell culture was mixed with 5 μL TMN containing 10 mM dithiothreitol and different amounts of NPE-caged-serine. The mixture was then introduced into a 10 μm-deep chamber and placed on an inverted microscope (model No. TE300; Nikon, Melville, NY), which is equipped with a charge-coupled device (CCD) camera (EM-CCD C9100; Hamamatsu, Hamamatsu City, Japan).

Flash photorelease and video microscopy

Our experimental setup is schematically depicted in Fig. 1. A light beam from the xenon arc lamp (75 W; Opti Quip, Highland Mills, NY) is controlled by an electronic shutter (Sutter Instrument, Novato, CA). The light passes through the standard epifluorescence microscopy attachment on the microscope and is introduced into the sample via a 20× objective. The fluorescence microscope is equipped with a 360 ± 40 nm excitation filter (Bio-Rad, Hercules, CA), a 400-nm dichroic mirror (Chroma Technology, Bellows Falls, VT), and a 510-nm long-pass emission filter (Chroma Technology). A convex lens was inserted behind the excitation filter so that a circular area (diameter ~2.5 mm) in the sample is uniformly illuminated by the UV light. In a typical experiment, the phase contrast images of the bacterial swimming trajectories were recorded at a 30 fps video rate for ~4 s before a 0.1-s UV pulse was applied. The video recording continued through the next 6 s. Because the diffusion constant of serine is $D = 900\ \mu m^2/s$ and only a very small area ~400 × 400 μm^2 in the center of the illuminated area is used for imaging, the serine concentration in this area can be considered constant during the measurement (8). Five sets of experiments were carried out with the released serine concentrations $c_0 \simeq 1$, 2.5, 5, 10, and 20 μM.

For each set of experiments, ~100 bacteria trajectories were analyzed. For the three-step swimmer *V. alginolyticus*, when the motor turns from CCW to CW, the cell body orientation is more or less the same. On the other hand, right after the motor turns from CW to CCW, the flagellum flicks, quickly deflecting the cell body to a new direction. Also, due to its proximity to surfaces, a bacterial swimming trajectory in the backward direction is usually more curved than in the forward direction (9). Based on the above features, most motor reversal events in a trajectory can be identified as either CCW-to-CW or CW-to-CCW transitions. Those reversals that cannot be identified without ambiguity can be determined based on the fact that CCW-to-CW and CW-to-CCW transitions occur alternatively. Very rarely is there more than one way to interpret the motor reversal sequence of a trajectory, and these trajectories are discarded. Once the type and time of the motor reversals for each bacterium are identified, the reversal probabilities $P_{f\to b}(t)$ and $P_{b\to f}(t)$ in the time interval $[t - \Delta t/2,\ t + \Delta t/2]$ can be calculated. The switching rates are then obtained: $k_f(t) = P_{f\to b}(t)/\Delta t$ and $k_b(t) = P_{b\to f}(t)/\Delta t$, where $\Delta t = 200$ ms. We noticed that for $c_0 = 20$ μM, almost all cells swim smoothly without motor reversal during the first second after the UV pulse, indicating that the bacterial response is already saturated. This concentration is therefore the maximal stimulation used in this work.

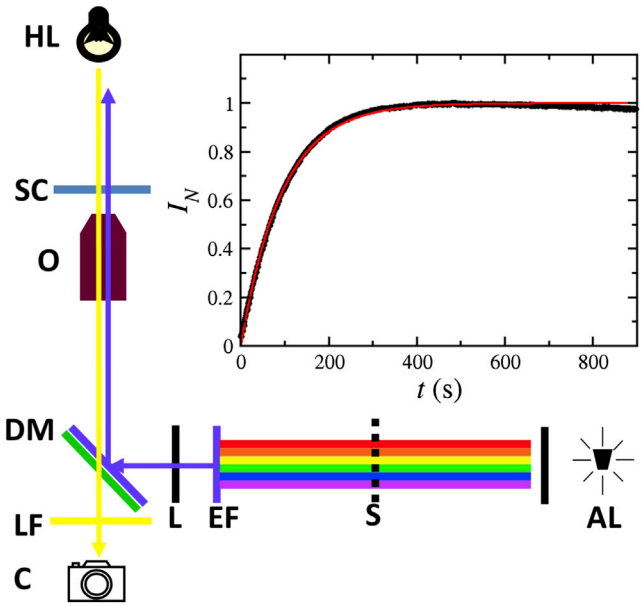

FIGURE 1 A schematic of experimental setup and the calibration curve for uncaging. The sample chamber (SC) is placed on an inverted microscope and illuminated by a halogen lamp (HL). Videos of bacterial trajectories are recorded through a 20× objective (O) with a CCD camera (C). The UV irradiation is set up via the epifluorescence attachment where light from an arc lamp (AL) passes through a UV band-pass excitation filter (EF) and a lens (L), and then is reflected into the objective (O) by a dichroic mirror (DM). An electronic shutter (S) is placed in front of the arc lamp and opens for 0.1 s to deliver the UV pulse. A 510-nm long-pass filter (LF) is used as the emission filter for HPTS. (*Inset*) Calibration of the release of serine using NPE-caged-HPTS is displayed by plotting the normalized fluorescence intensity, $I_N = I_{HPTS}/I_{HPTS}^{max}$, versus time t. (*Black dots*) Experimental datum; (*red curve*) theoretical fit to the equation $I_N = 1 - \exp(-kt)$. See main text for more details. To see this figure in color, go online.

Measured from the trajectories in the shallow chamber before the stimulation, the mean forward swimming duration is 0.43 s with a standard deviation of 0.34 s and the mean backward swimming duration is 0.50 s with a standard deviation of 0.23 s. In Xie et al. (2), the same quantities were measured in cells far from the surface. It was found that the mean forward swimming duration is 0.47 s with a standard deviation of 0.38 s and the mean backward swimming duration is 0.50 s with a standard deviation of 0.27 s. Therefore the effect of the cell-surface interaction on the switching rates is negligible.

Calibration of released serine upon exposure to a UV pulse

We used NPE-caged-HPTS to calibrate the amount of serine released in the experiment (10). HPTS is a fluorescent dye but is nonfluorescent when caged. When NPE-caged-HPTS is exposed to UV light, HPTS is released and can be excited in the wavelength range 340–380 nm, yielding the emission maximum at ~520 nm (10). To measure the uncaging efficiency of

NPE-caged-HPTS, 0.2 μL of 20 μM NPE-caged-HPTS in TMN was mixed with mineral oil by pipetting. This resulted in numerous oil-encapsulated NPE-caged-HPTS droplets that were stable for hours. Under the microscope, a droplet of diameter ~100–300 μm was chosen, and its fluorescence intensity was recorded at 1 fps for 15 min while the sample was continuously irradiated by the UV light as depicted in Fig. 1. The UV light uncages NPE-caged-HPTS as well as excites freed HPTS molecules.

In the inset of Fig. 1, normalized fluorescence intensity $I_N = I_{\mathrm{HPTS}}/I_{\mathrm{HPTS}}^{\max}$ as a function of time t is displayed, where $I_{\mathrm{HPTS}}^{\max}$ is the asymptotic maximum fluorescence intensity. As can be seen, I_N increases rapidly from $t = 0$ and reaches unity at $t \cong 500$ s when NPE-caged-HPTS is depleted. To quantify the measurement, we model uncaging kinetics using the first-order rate equation. The concentration of HPTS c_{free} in the droplet uncaged from NPE-caged-HPTS with an initial concentration of c_{caged} can be described as

$$\frac{dc_{\mathrm{free}}}{dt} = k\left(c_{\mathrm{caged}} - c_{\mathrm{free}}\right). \quad (1)$$

For the initial condition $c_{\mathrm{free}}(0) = 0$, the concentration of HPTS obeys $c_{\mathrm{free}}(t) = c_{\mathrm{caged}}(1 - \exp(-kt))$, and the fluorescent intensity $I_{\mathrm{HPTS}} \propto c_{\mathrm{free}}$. Because for $t > 500$ s, I_{HPTS} drops only ~2% by $t = 900$ s, a photobleaching term is not included in Eq. 1. By fitting the experimentally measured intensity to $I_N = 1 - \exp(-kt)$, we found $k = 1.07 \times 10^{-2}$ s^{-1}. The calibration procedure was repeated twice, resulting in $k = 1.00 \times 10^{-2}$ and 9.92×10^{-3} s^{-1}, yielding the mean uncaging rate of NPE-caged-HPTS to be $k = 10^{-2} \pm 5 \times 10^{-4}$ s^{-1}. This rate is proportional to the product of the extinction coefficient, which is mainly determined by the cage group, and the quantum yield, which is the probability of uncaging after absorption of a single photon. In our case, because both serine and HPTS are caged by the same NPE group, their extinction coefficients can be considered the same (11). According to Khan et al. (5) and Jasuja et al. (10), the quantum yield of NPE-caged-HPTS is 20 $\pm$ 4% of NPE-caged-serine. Taking into account the different light intensities used in the calibration and the measurements, we found that when the sample is exposed to the UV light for 0.1 s, ~1.0 $\pm$ 0.2% of NPE-caged-serine is uncaged.

RESULTS AND DISCUSSION

Responses of *V. alginolyticus* to stepwise chemoattractant stimuli

The bias of the flagellar motor switch

During chemotaxis, a bacterium actively modulates its motor rotation depending on external signals. For a two-state (CCW, CW) flagellar motor, a common way to characterize the switching behavior is the bias of the motor. In *E. coli*, for an example, when no external signal is present, individual flagellar motor rotates in the CCW direction ~70% of the time, and the bacterium spends ~90% of its time in the run mode (4,12). When an external signal is present, this interval is extended (shortened) if the run happens to be along (against) the chemoattractant gradient (12). The result is a biased random walk, causing the bacterium to drift toward the source of the attractant. The motor bias in polar flagellated bacterium *V. alginolyticus* has not been previously studied, and below we report observations that reveal important differences from *E. coli*.

We first focus on population statistics of flagellar motor bias when a stepwise chemoattractant stimulus is applied. Individual cells are tracked for up to 4 s before and 6 s after the stimulation. Four typical bacterial trajectories are displayed in Fig. 2. It is found that in response to the stepwise stimulus, the bacteria extend their swimming intervals regardless of their motor directions, suggesting that unlike peritrichously flagellated bacteria, such as *E. coli, Salmonella typhimurium*, and *Bacillus subtilis*, the polar flagellated bacterium *V. alginolyticus* can perform chemotaxis

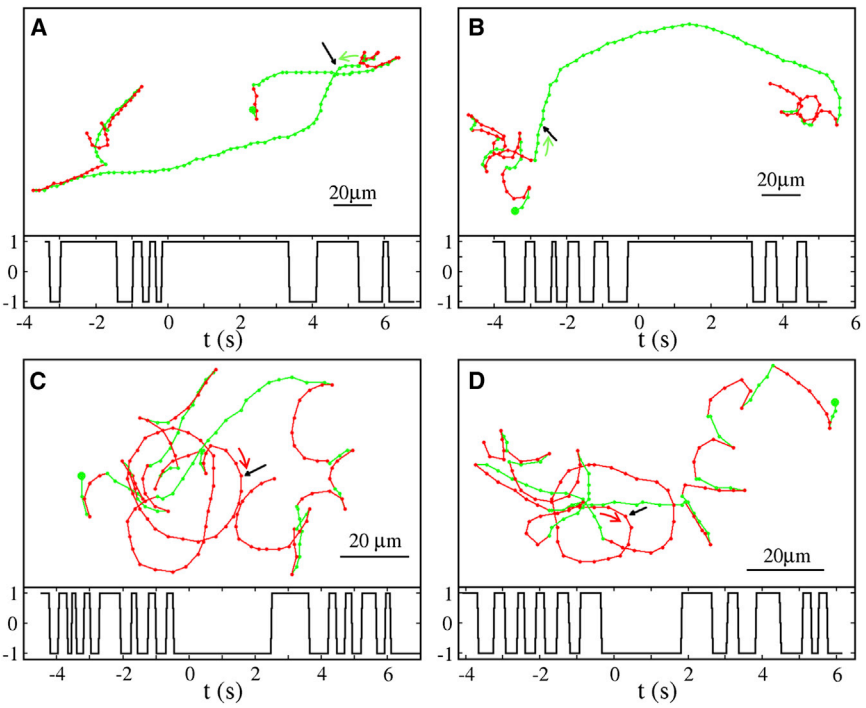

FIGURE 2 Bacterial tracks before and after a stepwise stimulus. The top panels (*A* and *B*) show two bacterial trajectories when the cells are stimulated while swimming forward or in the CCW motor state. The bottom two panels (*C* and *D*) show two bacterial trajectories when the cells are stimulated while swimming backward or in the CW motor state. The stepwise stimulation is applied at $t = 0$ (see the *black arrows*) when 20 μM serine is photoreleased into the medium. (*Green* and *red curves*) Forward and backward swimming segments, respectively; (*large green dots*) starting points of the trajectories; and (*small green* and *red dots*) positions of the cells at an equal time interval of 0.067 s, respectively. (*Green arrows* in *A* and *B* and *red arrows* in *C* and *D* indicate the cells' movement directions right before stimulation.) Because the chamber is shallow, ~10 μm deep, hydrodynamic interactions between the cells and the glass surface cause the backward swimming segments (*red*) to curve more strongly than the forward ones (*green*). For each bacterium, a binary time trace (1 for forward and −1 for backward) can be constructed and is displayed directly beneath each trajectory (see text for more details). To see this figure in color, go online.

and actively pursue a chemical gradient in both swimming directions. To facilitate quantitation of such a response, cells were grouped into two classes depending on their motor rotation states at the moment of stimulation: The subpopulation that swims in the forward direction (or with a CCW motor) at $t = 0$ is labeled as a plus-symbol (+) and the subpopulation that swims in the backward direction (or with a CW motor) at $t = 0$ is labeled as a minus symbol (−).

Each bacterial trajectory is then described by a binary function of time. In detail, the trajectory of the ith cell that belongs to the plus-symbol subpopulation is designated as $n_i(t|+) = +1$ if the cell is going forward at time t and $n_i(t|+) = -1$ if the cell is going backward at time t. Similarly, $n_i(t|-)$ can be constructed for cells that swim in the backward direction at time $t = 0$. In Fig. 2, these time traces, $n_i(t|+)$ and $n_i(t|-)$, are presented in the lower panels of their corresponding trajectories. These traces make clear that elongation of the swimming intervals after a stepwise stimulation (20 μM serine) is statistically very significant.

For a systematic study, different concentrations of serine c_0 were used, corresponding to $c_0 \simeq 1$, 2.5, 5, 10, and 20 μM, and $N \sim 50$ cells were tracked for each subpopulation. Fig. 3 shows the bias function

$$B_{\pm}(t) \equiv \sum_{i=1}^{N} n_i(t|\pm)/N$$

as a function of time when cells are stimulated at $t = 0$. By this definition, initially $B_{\pm}(t = 0) = \pm 1$ and over time $B_{\pm}(t)$ decay to zero, meaning that half of the subpopulation swims forward and the other half backward. This is also true for $t \leq 0$, as delineated in Fig. 3, *A–F*, indicating that in the absence of chemical cues, or in a steady state, there is no preferred motor direction in the subpopulations. Thus, $B_+(t)$ ($B_-(t)$) is the conditional probability that a cell swims in the forward (backward) direction at time t given that it is in the forward (backward) direction at $t = 0$. Fig. 3 *A* indicates that in the steady state where there is no chemical stimuli, bias decays very rapidly with a time constant ~0.2 s. This fast decay is a result of random, spontaneous motor reversals and provides a baseline for further analysis.

The situation is quite different when a chemical signal is present ($t > 0$) as illustrated by Fig. 3, *B–F*. This motor state, either forward or backward, is extended by the stimulation, and the persistent time gets longer as the stimulation level increases. The data also show that for a sufficiently long time, $B_{\pm}(t)$ decays to zero, indicating that the bacterium is able to adapt to the new level of attractant in both swimming directions. It should be mentioned that for most of serine concentrations used, the stepwise stimulation elicits a stronger response in the forward intervals than the backward ones, i.e., there is a greater persistence in forward than in backward swimming after stimulation. Quantitatively, this can be seen in Fig. 3, *B–E*, where $B_-(t)$ in general decays faster than $B_+(t)$. Interestingly, however, this difference appears to diminish as c_0 increases, as delineated in Fig. 3 *F*, where $B_-(t)$ and $B_+(t)$ become almost symmetric for $c_0 = 20$ μM.

The switching rates k_f and k_b of the flagellar motor switch

The more fundamental quantities characterizing flagellar motor switches are the time-dependent switching rates,

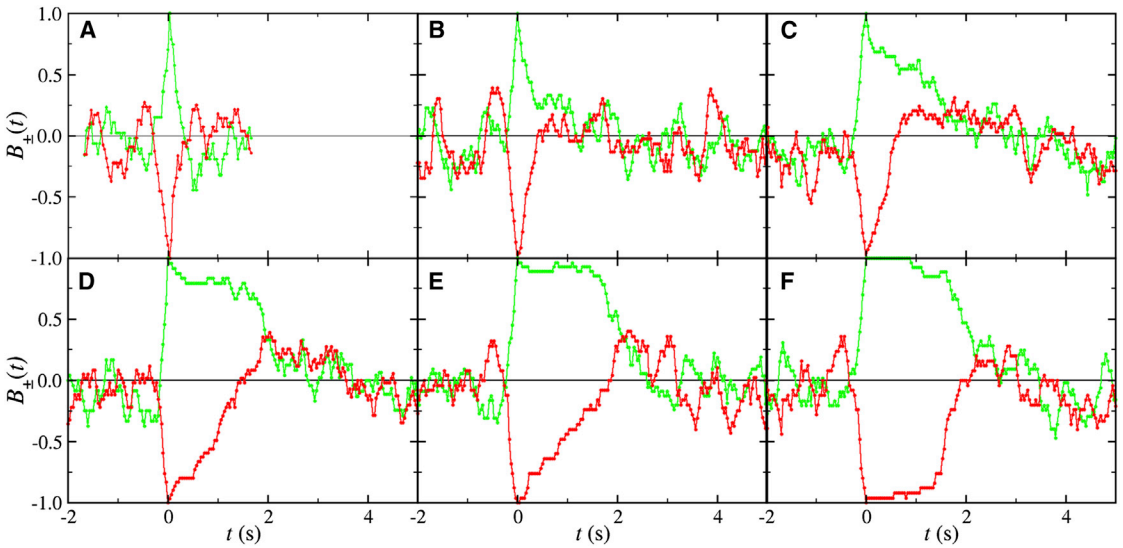

FIGURE 3 Persistence in motor bias of the flagellar motor upon a stepwise stimulation. (*A*) Persistence in motor bias when there is no chemical stimulus; (*B–F*) persistence in motor bias after different levels of chemical stimuli ($c_0 \simeq 1$, 2.5, 5, 10, and 20 μM) were administrated at $t = 0$. The green (*red*) curves are for $B_+(t)$ ($B_-(t)$), representing the persistence in the bias of the subpopulation that is swimming forward (backward) at $t = 0$. The measurements showed that before and long after the stimulation, the bacteria do not have a preferred swimming direction, giving $B_{\pm}(t < 0) \simeq B_{\pm}(t > 3\text{ s}) \simeq 0$. On the other hand, immediately after the stimulation, the cells significantly prolong their motor rotation state, resulting in slow decay of $B_{\pm}(t)$. To see this figure in color, go online.

$k_f(t)$ and $k_b(t)$, i.e., the probability per time that a bacterial flagellar motor makes the transition from CCW to CW rotation and from CW to CCW, respectively. Fig. 4 displays these time-dependent rates when the bacteria are stimulated with different c_0. For $t < 0$, both k_f and k_b fluctuate around the steady-state switching rates $k_{f0} \simeq 2.3 \pm 0.1\ s^{-1}$ and $k_{b0} \simeq 1.9 \pm 0.1\ s^{-1}$, which are delineated by the blue dashed lines in the plots. Three features were observed.

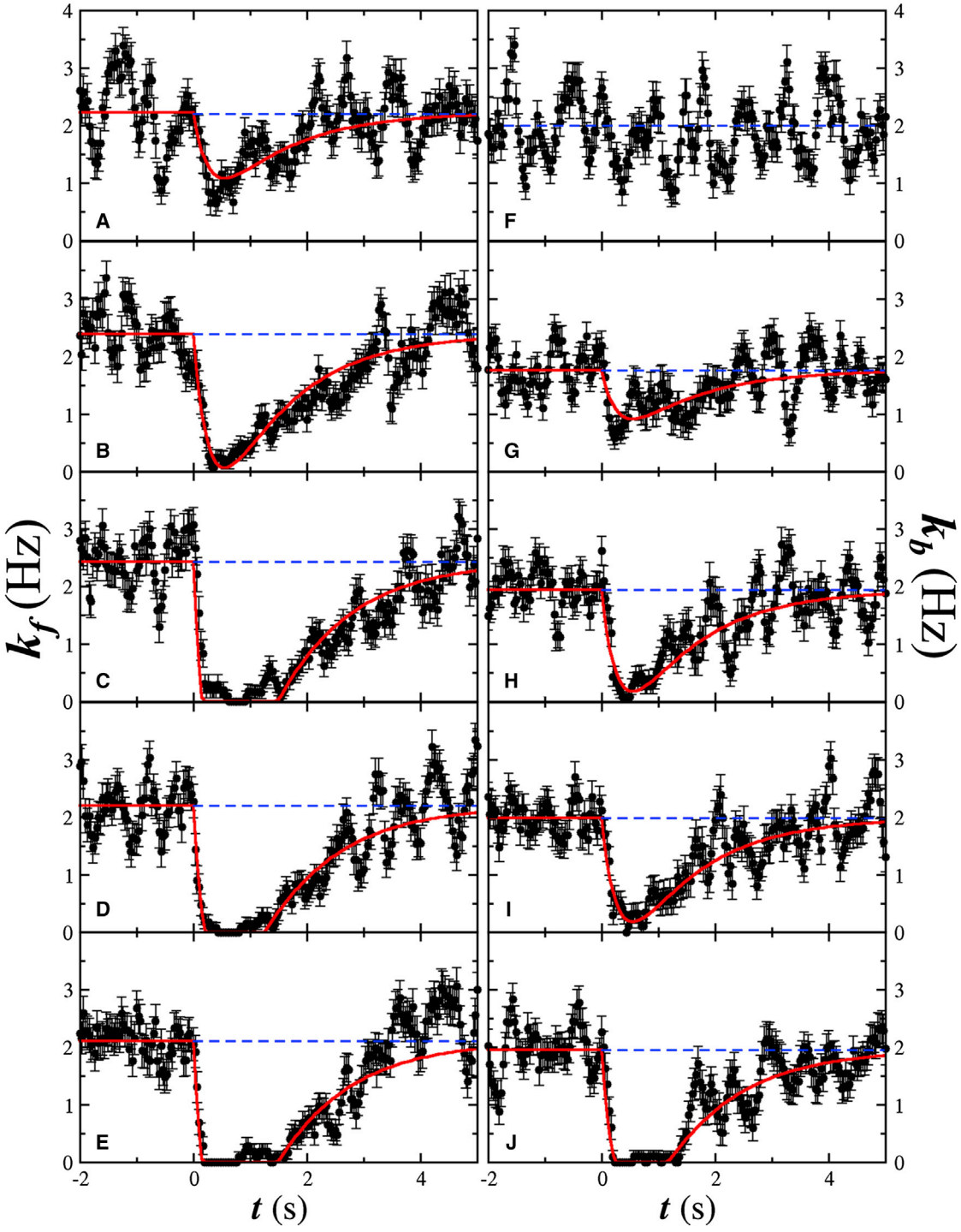

FIGURE 4 Flagellar motor switching rates $k_f(t)$ and $k_b(t)$ resulting from a stepwise stimulus. (*A–E*) The value $k_f(t)$ before and after the ambient serine concentration jumps from 0 to $c_0 = 1$, 2.5, 5, 10, and 20 μM, respectively. (*F–J*) The value $k_b(t)$ before and after the ambient serine concentration jumps from 0 to $c_0 = 1$, 2.5, 5, 10, and 20 μM, respectively. (*Blue dashed line*) Average prestimulation rates k_{f0} and k_{b0}, respectively. (*Red curves*) Fitting results using Eq. 6. To see this figure in color, go online.

1. Both k_f (Fig. 4, *A–E*) and k_b (Fig. 4, *F–J*) recover the prestimulation levels for a sufficiently long time. This shows that, for the given range of c_0, the chemotaxis network of *V. alginolyticus* adapts nearly perfectly to serine. Such a behavior is similar to *E. coli*'s response to aspartate but not to serine; the latter was found to be imprecisely adaptive at concentrations higher than 1 μM (12).
2. Shortly after stimulation, both k_f and k_b decrease as a result of exposure to serine, and the amplitude of the responses correlates strongly with c_0. For a relatively high-level serine stimulus, such as $c_0 = 20$ μM (see Fig. 4, *E–J*), the decrease in the switching rates can be greater than their steady-state values. As a result, k_f and k_b remain zero for some time (~1 s) before rising toward the prestimulation value.
3. For a low-level stimulus, the responses in the forward and backward directions are not symmetrical. For example, in the case of $c_0 = 1$ μM, while $k_f(t)$ drops significantly by ~1.5 Hz, little change is seen in $k_b(t)$. This suggests that the flagellar motor in the CW state is less sensitive to the change in the regulator protein (CheY-P) concentration than its CCW counterpart (see more discussion below). However, this asymmetry appears to disappear when the stimulation level is increased. This behavior is similar to what is observed in the previous subsection.

The above rate measurements reveal an important difference between *V. alginolyticus's* and *E. coli*'s response to a chemoattractant stimulus: While both microorganisms reduce the motor switching rate when it is in the CCW state, the response of a CW-rotating motor is exactly opposite in the two organisms, i.e., while k_b is reduced in *V. alginolyticus*, the corresponding rate in *E. coli* is increased (13). From the standpoint of a microorganism, both responses make good sense. Because *V. alginolyticus* is a bidirectional swimmer and able to pursue chemoattractant in both forward and backward swimming directions, by extending the backward swimming interval when positively stimulated, the cell can migrate closer to the source of attractant. On the other hand, because the CW state cannot produce displacement for *E. coli*, quickly switching out of that state upon being positively stimulated so that the cell can pursue new opportunities also makes good biological sense. However, how the microorganisms use the essentially identical set of regulatory proteins to achieve this remarkable feat is fascinating and remains to be investigated.

Theoretical interpretations

Modeling the chemotaxis response of V. alginolyticus

Based on extensive experimental data on the chemotaxis network of *E. coli*, a concise mathematical model was proposed by Tu et al. (14). In their work, the cooperativity among chemoreceptors is described by the MWC model, where the activity a of the kinase CheA ($0 \le a \le 1$) is determined by the methylation-dependent free energy f_m, and the attractant-binding-dependent free energy f_c. Denoting the dissociation constants of inactive and active forms of receptors as K_I and K_A, they found $f_c(c) = \ln[(1 + c/K_I)/(1 + c/K_A)]$, where c is the chemoattractant concentration. Taking into account the biochemical interactions among different regulatory proteins, the model predicts the output of the chemotaxis network, i.e., the CheY-P concentration fluctuations around the equilibrium value $[YP]_0$, $\Delta[YP] \equiv [YP] - [YP]_0$, with the result

$$\Delta[YP](t) = \int^{t} R_Y(t - t')\Delta f_c(t')dt', \tag{2}$$

where Δf_c is the deviation of f_c from its prestimulation value, and $R_Y(t)$ is the response function of $[YP]$ given by

$$R_Y(t>0) = R_{Y0}[\tau_z \exp(-t/\tau_m) - \tau_m \exp(-t/\tau_z)]/(\tau_m - \tau_z). \tag{3}$$

Here, τ_m and τ_z are, respectively, the methylation and dephosphorylation times, and $R_{Y0} = Na_0(1 - a_0)k_a$ is the gain of the response, which depends on the equilibrium activity a_0 of CheA, the number N of subunits in the chemoreceptor cluster, and the effective phospho-transfer rate k_a from CheA to CheY.

Compared to the chemotaxis system of *E. coli*, much less is known about the biochemical processes in *V. alginolyticus*. However, progress can still be made because of conservation of gene sequences and protein functions. Comparative studies have shown that at the receptor level, although *E. coli* has only five methyl-accepting chemotaxis proteins or (in short) chemoreceptors, there are more than 20 putative methyl-accepting chemotaxis proteins in *V. alginolyticus*. Despite such differences, organization of receptors in diverse bacterial species is remarkably the same. Namely, functional receptors tend to cluster around poles of a cell body and the cluster size can be remodeled by external signals (15,16). This suggests that in different bacteria, receptors function by forming arrays to promote cooperativity and to increase their sensitivity. The mathematical formulation of $f_c(c)$ for *E. coli* is therefore expected to be applicable to other bacteria including *V. alginolyticus*.

At the regulation level, *V. alginolyticus* has all six core chemotaxis proteins of *E. coli,* Che(ABRWYZ). Two exceptions are as follows.

1. *V. alginolyticus* possesses CheV, a chemotaxis protein that is also identified in other bacterial species and involved in adaptation (17).
2. *V. alginolyticus* appears to have an additional putative CheY coded by a gene remote from all other *che* genes on the bacterial chromosome.

A study in our lab found that once the canonical copy of *cheY,* which is between *cheZ* and *fliA*, in the strain YM4 was deleted, the cell cannot respond to either chemoattractant or chemorepellent, indicating that the gene product of this *cheY* is the only chemotaxis response regulator in YM4 that interacts with the polar flagellar motor. This observation is consistent with an earlier study demonstrating that this canonical copy of CheY controls both the polar and lateral flagellar motor switches (18). And the six *che* genes *(cheA*, *B*, *R*, *W*, *Y*, and *Z*) in *V. alginolyticus* share significant homology with those of *E. coli*, suggesting that their functions in the chemotaxis network are similar as well. For example, 84% of the amino acids of *V. alginolyticus*' CheY protein are identical to those of *E. coli*. Moreover, the functional sites, such as the sites for phosphorylation and motor docking of these two CheY proteins, are almost identical, suggesting that *V. alginolyticus*' CheY and *E. coli*'s CheY may be interchangeable (18). Hence, below we will assume that Eq. 2 can also be used to describe concentration fluctuations of $[YP]$ in *V. alginolyticus* in response to a chemical stimulus.

Recently, we characterized the switching behavior of the polar flagellar motor of *V. alginolyticus* and found that in contrast to *E. coli*'s flagellar motor, an increase in $[YP]$ increases both k_f and k_b (L. X., J. He, T. Altindal, and X.-L. Wu, unpublished data). Specifically, around the physiological concentration $[YP]_0$, $k_f([YP])$ and $k_b([YP])$ can be described as

$$k_x([YP]) = k_{x0}\left(1+\frac{H_x}{[YP]_0}\left([YP]-[YP]_0\right)\right), \qquad (4)$$

where $x \in \{f, b\}$, and H_x is a gain factor of the motor. Combining Eqs. 2 and 4, the response of k_f and k_b to a chemical stimulation can be written as

$$k_x(t) = k_{x0}\left(1+\frac{H_x}{[YP]_0}\int^t R_Y(t-t')\Delta f_c(t')dt'\right). \qquad (5)$$

In our experiment, cells were suspended in the motility buffer and a fixed amount of serine was released by the photolabile compound during a short interval of 0.1 s. Because free serine was created over a sufficiently large area, we expect

$$c(t) = \begin{cases} 0 & t\le 0 \\ c_0 & t>0, \end{cases}$$

which gives $\Delta f_c = \ln[(1 + c_0/K_I)/(1 + c_0/K_A)]$ for $t > 0$. Replacing this result in Eq. 5 yields

$$k_x(t) = k_{x0}\left[1-R_{x0}\frac{\tau_Z\tau_m}{\tau_m-\tau_Z}\left(\exp\left(-\frac{t}{\tau_m}\right)-\exp\left(-\frac{t}{\tau_Z}\right)\right)\right], \qquad (6)$$

where $R_{x0} = H_xR_{Y0}\Delta f_c/[YP]_0$ is the overall chemotaxis response amplitude.

Comparisons with the experimental observations

To extract quantitative information for the chemotactic network of *V. alginolyticus* using the above theoretical model, curves in Fig. 4 were fitted using Eq. 6. To minimize the number of free parameters, the steady-state switching rates k_{f0} and k_{b0} are assumed to be known, determined by averaging $k_f(t)$ and $k_b(t)$ from $t = -2$ s to $t = 0$ s. The remaining constants in Eq. 6, such as R_{x0}, τ_z, and τ_m, are treated as adjustable parameters. To account for the saturation in responses at $c_0 = 10$ and 20 μM, where $k_f(t)$ or $k_b(t)$ remains zero for >1 s, parameters that cause $k_x(t)$ to be negative are allowed, but negative $k_x(t)$ is replaced by zero. Within the linear-response approximation, τ_z and τ_m are expected to be independent of c_0 and should be treated as global fitting parameters. As shown by the red lines in Fig. 4, the quality of the fits is satisfying, considering that effectively R_{x0} is the only local fitting parameter for each curve. The nonlinear regression procedure yields $\tau_m = 1.29 \pm 0.04$ s and $\tau_m = 0.28 \pm 0.01$ s. These chemotactic timescales in the marine bacterium are considerably shorter compared to those observed in *E. coli* (4,14).

As for the response amplitudes, it was found that $R_{f0} = 2.8 \pm 0.6$, 5.2 ± 0.6, 8.8 ± 1.2, 7.5 ± 0.9, and 8.9 ± 1.2 Hz for the forward intervals (see Fig. 4, *A–E*), corresponding to $c_0 = 1$, 2.5, 5 10 and 20 μM, respectively, and that $R_{b0} = 2.6 \pm 0.6$, 4.9 ± 0.6, 4.9 ± 0.6, and 7.1 ± 0.9 Hz for the backward intervals (see Fig. 4, *G–J*), corresponding to $c_0 = 2.5$, 5, 10, and 20 μM, respectively. In Fig. 5, the amplitudes of the responses, R_{f0} (*green squares*) and R_{b0} (*red dots*), are plotted for different serine concentrations c_0. Here both curves appear linear when c_0 is plotted on a semilogarithmic scale, indicating that chemical sensing of the marine bacterium obeys Weber's law, like many other biological systems (19). Moreover, from these measured response amplitudes, the binding affinity (or the association constant) K_I between serine and the chemoreceptors can be estimated because R_{x0} is linear in $\Delta f_{(c)} = \ln[(1 + c/K_I)/(1 + c/K_A)]$, which can be

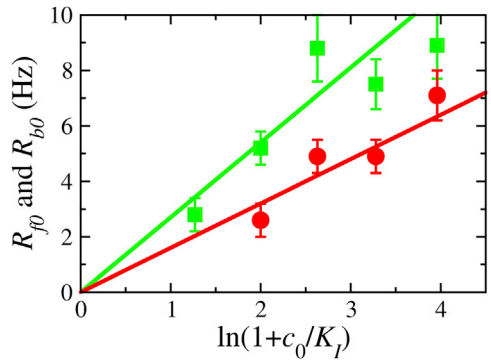

FIGURE 5 Response amplitudes R_{f0} and R_{b0} as a function of c_0. (*Green squares* and *red dots*) The measured R_{f0} and R_{b0}, respectively. (*Green* and *red lines*) Fitting results for R_{f0} and R_{b0} using $R_{x0} = \ln(1 + c_0/K_I) \times H_xR_{Y0}/[YP]_0$, respectively. To see this figure in color, go online.

approximated as $\Delta f_c \approx \ln(1 + c_0/K_I)$ when $K_A \gg c_0$. By fitting the amplitudes to $R_{x0} = \ln(1 + c_0/K_I) \times H_x R_{Y0}/[YP]_0$ as shown in Fig. 5, the binding affinity is found to be $K_I \approx 0.39 \pm 0.25$ μM, $H_f R_{Y0}/[YP]_0 = 2.7 \pm 0.6$ Hz, and $H_b R_{Y0}/[YP]_0 = 1.6 \pm 0.4$ Hz. Because R_{Y0} and $[YP]_0$ are parameters of the chemotaxis network that are independent of the motor state, the ratio of the above slopes yields immediately $H_f \simeq 1.7\ H_b$. Thus, around the physiological $[YP]_0$, the gain of the motor in the CCW state is nearly twice of that in the CW state. The most likely possibility for this difference is that the motor switch has a higher sensitivity to the regulator protein CheY-P when in the CCW state than in the CW state.

A possible biophysical reason for asymmetric flagellar motor response

Although it is difficult to know exactly why there is an asymmetry in the response of the cell in the forward and backward swimming intervals, its motility pattern may provide some clue. In the presence of a chemical gradient, it may be more advantageous to break the symmetry. Note that due to the flick that randomizes cell orientations, a forward displacement cannot retrace the previous backward trajectory but when the cell switches from forward to backward swimming, the cell can backtrack the previous forward trajectory. As a result, if the cell moves down the gradient during a forward run it can revisit the more favorable pasture by reversing its motor. However, if the backward swimming is in the unfavorable direction, a motor reversal is highly unlikely to orient the cell into the favorable direction. Therefore, forward and backward swimming intervals are not equivalent; the forward swimming is more suitable for exploration but the backward swimming is more suitable for exploitation or localization. Hence, when stimulated by an attractant, k_f should have a stronger response than k_b so that the cell can locate a nutrient source with a weak gradient. An alternative way to illustrate the advantage of the asymmetry is by analyzing the drift velocity v_d in a linear gradient. Combining Eq. 7 in Altindal et al. (20) with Eq. 6, it can be shown that

$$v_d = \frac{v^2 \nabla f_c \tau_0^2 \tau_z \tau_m}{6(\tau_0 + \tau_z)(\tau_0 + \tau_m)} \left(R_{f0} - R_{b0} \frac{\tau_z \tau_m - \tau_0^2}{(\tau_0 + \tau_z)(\tau_0 + \tau_m)} \right), \tag{7}$$

when $k_{f0} \simeq k_{b0} \simeq {\tau_0}^{-1}$, which is a good approximation for YM4. In the above, v is the bacterial swimming speed, $\tau_0 \simeq 0.5$ s is the average swimming interval, and $\tau_z \simeq 0.3$ s and $\tau_m \simeq 1.3$ s are the phosphorylation and methylation times, respectively, according to our measurements. In the limit $K_I \ll c \ll K_A$,

$$\nabla f_c \simeq \nabla \ln(c) \simeq \nabla c/\bar{c},$$

where $\bar{c}$ can be considered the local chemical concentration to which the bacteria adapt. We note that because $\tau_z \tau_m - {\tau_0}^2 > 0$, the second term in the bracket is negative. This negative term results from the memory effect in chemo-sensing during backtracking, because the gradient sensed by the cell could be opposite to the one it currently experiences (20,21). Therefore, if a large v_d is desired for chemotaxis, Eq. 7 shows that a large R_{f0} and a relatively small R_{b0} is beneficial.

CONCLUSIONS

This work addresses the intriguing issue of how a marine bacterium regulates its polar flagellar motor switch in chemotaxis. Why is this switch regulated in a different manner compared to *E. coli*? From a biological perspective, these two bacteria have the same basic need of migrating in a chemical gradient rapidly, but their motility patterns are distinctively different: The marine bacterium can swim bidirectionally but the enteric bacterium swims when the motor is in the CCW state; the CW state is reserved for a different function to randomize the swimming direction. The important question then is how cells remodel their regulatory machineries (i.e., the software) to match their motility apparatus (i.e., the hardware) in order to achieve the optimal chemotactic behavior. Via a stepwise stimulation, our work demonstrates the following.

1. The significant difference in the motility apparatuses of the two bacteria completely reverses the input-output relationship of the chemotaxis response when the motor is in the CW state. Specifically, for *V. alginolyticus*, a positive stimulus reduces the switching rate k_b of the CW state in the same way as it reduces k_f of CCW state. This is exactly the opposite to *E. coli* (13).
2. It is noteworthy that the difference in the swimming speeds of these two bacterial species is reflected in the difference of their response timescales of the chemotaxis network. Specifically, we found that τ_z and τ_m in *V. alginolyticus* are approximately one-half of those found in *E. coli* (4,14). In oceans, *V. alginolyticus* swims at a speed of ~100 μm/s, much higher than *E. coli.* When detecting a chemical gradient by temporal sensing, a higher swimming speed requires a shorter processing time so that the cell can respond swiftly and does not drift in an unfavorable direction for too long.

The emerging picture of how *V. alginolyticus* coordinates its motility pattern for chemotaxis is the following: Similar to *E. coli*, when the marine bacterium migrates up an attractant gradient, an increasing binding of the attractant to the receptor reduces CheA activity, resulting in a decline of $[YP]$ inside the cell. The decrease in $[YP]$ leads to a reduction in both switching frequencies, k_f and k_b, so that the cell can persist in its direction regardless of the motor state. On the other hand, if the cell descends an attractant gradient, the above process reverses so that the cell is more likely to reverse the motor direction by increasing the switching

frequencies, k_f and k_b, again regardless of its motor states. Despite their contrasting motility patterns, therefore, *V. alginolyticus* and *E. coli* achieve the same chemotaxis goal by extending runs in the favorable direction and cutting short those in the unfavorable direction. As a result, both of them are able to migrate toward an attractant source using a biased random walk.

A large class of marine bacteria has a single polar flagellum powered by a bidirectional flagellar motor similar to *V. alginolyticus*. Due to low-Reynolds-number hydrodynamics, the motility patterns of these bacteria are likely to be run-reverse or run-reverse-flick for which some evidence is already available (2,22). The chemotactic response of *V. alginolyticus* is well suited for this class of bacteria. However, whether these bacteria adopt this unique response is an open question but can be answered by future experiments. In these experiments one expects to observe that symmetry in the chemotaxis response is tied to the symmetry in the motility pattern, e.g., in the completely symmetrical case where a cell does not differentiate forward and backward swimming, which requires no flicking, the symmetry in the responses in the two motor states should be completely restored.

AUTHOR CONTRIBUTIONS

L.X. and X-L.W. designed research, performed research, analyzed data, and wrote the paper. C.L. contributed experimental material and wrote the paper.

ACKNOWLEDGMENTS

We thank Prof. Paul Floreancig from the Department of Chemistry at the University of Pittsburgh, in whose lab the NPE-caged-serine is synthesized.

The work is supported by the National Science Foundation under grant No. DMR-1305006.

REFERENCES

1. Son, K., J. S. Guasto, and R. Stocker. 2013. Bacteria can exploit a flagellar buckling instability to change direction. *Nat. Phys.* 9:494–498.
2. Xie, L., T. Altindal, …, X.-L. Wu. 2011. Bacterial flagellum as a propeller and as a rudder for efficient chemotaxis. *Proc. Natl. Acad. Sci. USA.* 108:2246–2251.
3. Altindal, T., S. Chattopadhyay, and X.-L. Wu. 2011. Bacterial chemotaxis in an optical trap. *PLoS ONE.* 6:e18231.
4. Segall, J. E., S. M. Block, and H. C. Berg. 1986. Temporal comparisons in bacterial chemotaxis. *Proc. Natl. Acad. Sci. USA.* 83:8987–8991.
5. Khan, S., F. Castellano, …, D. R. Trentham. 1993. Excitatory signaling in bacterial probed by caged chemoeffectors. *Biophys. J.* 65:2368–2382.
6. Kawagishi, I., Y. Maekawa, …, Y. Imae. 1995. Isolation of the polar and lateral flagellum-defective mutants in *Vibrio alginolyticus* and identification of their flagellar driving energy sources. *J. Bacteriol.* 177:5158–5160.
7. Tokuda, H., T. Nakamura, and T. Unemoto. 1981. Potassium ion is required for the generation of pH-dependent membrane potential and ΔpH by the marine bacterium *Vibrio alginolyticus*. *Biochemistry.* 20:4198–4203.
8. Ma, Y., C. Zhu, …, K. T. Yu. 2005. Studies on the diffusion coefficients of amino acids in aqueous solutions. *J. Chem. Eng. Data.* 50:1192–1196.
9. Magariyama, Y., M. Ichiba, …, T. Goto. 2005. Difference in bacterial motion between forward and backward swimming caused by the wall effect. *Biophys. J.* 88:3648–3658.
10. Jasuja, R., J. Keyoung, …, S. Khan. 1999. Chemotactic responses of *Escherichia coli* to small jumps of photoreleased L-aspartate. *Biophys. J.* 76:1706–1719.
11. Sarkisov, D. V., and S. S. H. Wang. 2006. Alignment and calibration of a focal neurotransmitter uncaging system. *Nat. Protoc.* 1:828–832.
12. Berg, H. C., and D. A. Brown. 1972. Chemotaxis in *Escherichia coli* analyzed by three-dimensional tracking. *Nature.* 239:500–504.
13. Block, S. M., J. E. Segall, and H. C. Berg. 1982. Impulse responses in bacterial chemotaxis. *Cell.* 31:215–226.
14. Tu, Y., T. S. Shimizu, and H. C. Berg. 2008. Modeling the chemotactic response of *Escherichia coli* to time-varying stimuli. *Proc. Natl. Acad. Sci. USA.* 105:14855–14860.
15. Gestwicki, J. E., A. C. Lamanna, …, J. Adler. 2000. Evolutionary conservation of methyl-accepting chemotaxis protein location in bacteria and archaea. *J. Bacteriol.* 182:6499–6502.
16. Bray, D., M. D. Levin, and C. J. Morton-Firth. 1998. Receptor clustering as a cellular mechanism to control sensitivity. *Nature.* 393:85–88.
17. Alexander, R. P., A. C. Lowenthal, …, K. M. Ottemann. 2010. CheV: CheW-like coupling proteins at the core of the chemotaxis signaling network. *Trends Microbiol.* 18:494–503.
18. Kojima, M., R. Kubo, …, I. Kawagishi. 2007. The bidirectional polar and unidirectional lateral flagellar motors of *Vibrio alginolyticus* are controlled by a single CheY species. *Mol. Microbiol.* 64:57–67.
19. Mesibov, R., G. W. Ordal, and J. Adler. 1973. The range of attractant concentrations for bacterial chemotaxis and the threshold and size of response over this range. Weber law and related phenomena. *J. Gen. Physiol.* 62:203–223.
20. Altindal, T., L. Xie, and X.-L. Wu. 2011. Implications of three-step swimming patterns in bacterial chemotaxis. *Biophys. J.* 100:32–41.
21. de Gennes, P. G. 2004. Chemotaxis: the role of internal delays. *Eur. Biophys. J.* 33:691–693.
22. Taylor, B. L., and D. E. Koshland, Jr. 1974. Reversal of flagellar rotation in monotrichous and peritrichous bacteria: generation of changes in direction. *J. Bacteriol.* 119:640–642.